Particle size and fraction required to stabilise aluminium alloy foams created by gas injection

K. Heim[1,2], F. García-Moreno[1,2], J. Banhart[1,2]

[1]Technische Universität Berlin, Hardenbergstraße 36, 10623 Berlin, Germany

[2]Helmholtz-Zentrum Berlin, Hahn Meitner Platz 1, 14109 Berlin, Germany

Liquid metal foam owes its stability to the presence of solid non-metallic particles. To elucidate the conditions under which such particles stabilise foams, 15 different aluminium-alloy based metal matrix composites were manufactured and melted, after which air was injected with the objective to create bubbles and eventually metal foam. Bubble and foam formation was monitored in-situ by X-ray radioscopy. All systems were classified and labelled *foamable*, *partially foamable* and *unfoamable*. Foamable composites form a preferred range in the stability diagram displaying particle fractions vs. particle size, thus experimentally confirming earlier claims. All investigated composites fall into the same range even though their alloy compositions and particle types vary.

Keywords: Al-foams, composites, particle stabilised, X-ray imaging

The most direct way to create a metal foam is to inject gas into a molten alloy. While this idea occurs already in a very early patent [1] details on processing were disclosed and the importance of foam stabilisation discovered only many years later, as reviewed in Ref. [2]. It is now known that a dispersion of non-metallic particles in a liquid alloy is a pre-requisite for growing foam. Such particles decorate bubble/metal interfaces and prevent two bubbles that come into contact with each other from forming a bigger joint bubble. How exactly particles prevent coalescence is not known in detail and some controversy remains [3-5].

The conditions under which an alloy can be foamed by particles have been investigated for the important system Al-Si/SiC. Originally, this particle-reinforced metal matrix composite was developed as an alloy with improved mechanical properties, but during processing in the liquid state its foamability was discovered. The ability of SiC particles of various diameters and volume fractions to keep foam stable was investigated and a preferred

range identified. However, the particle fraction vs. particle size stability diagram published in a patent [6] is only schematic and not based on documented experiments (although some might have been carried out). Aluminium alloy melts containing varying contents of stabilising SiC particles have been studied to determine the particle fraction required to create stable foams by gas injection [3]. Other studies concentrated on important parameters such as the particle size [7] immersion depth of the gas injector [8], type of blowing gas [9], or injection conditions [10].

The aim of this paper is to provide an experimental proof of the stability diagram suggested in Ref. [6]. As no series of composites with a wide range of different particle sizes is available, we chose different alloys stabilised with different particles, in total 15. They represent a wide range of particle size vs. particle fraction combinations. We monitor the formation of liquid metal foam in-situ by X-ray radioscopy and distinguish between various levels of foamability. The result of the study is the confirmation of the stability diagram and the finding that it does not sensitively depend on the type of metal matrix composite.

Composite F3S20S produced by Alcan, Montréal, Canada, containing 20 vol.% SiC particles of 10 µm mean diameter embedded in an alloy AlSi9Mg0.6 (in wt.%) was considered a reference material in this work due to its known foamability, see Figure 1 and Table 1, #2. All the composites prepared in the present study are based on alloy AlSi9Mg0.6. The foamable materials prepared can be divided into three categories depending on how they are manufactured: (i) Composites are called *extrinsic* ('Ex') when they contain particles that were added to a melt from the outside. Beside SiC particles, Al_2O_3 or SiO_2 have been used as extrinsic particles [8,11-14]. Composites are manufactured by adding powders to the vortex in the melt while stirring at 1000 rpm. (ii) Composites are called *intrinsic* ('In') whenever particles are formed by reactions inside the liquid alloys. Such particles are produced by adding oxidants such as SiO_2 and CuO to create Al-based oxides (Al_2O_3, Al_2MgO_4 (spinel) or Al-Mg-O transition phases) and by a flux-assisted synthesis route leading to the formation of TiB_2 particles [15]. (iii) Some composites contain *primary* crystals that are formed in the first stage of solidification of eutectic alloys. Primary Fe and Si-rich crystals were obtained after modifying the basic alloy AlSi9Mg0.6 by addition of 3 wt.% Fe or 11 wt.% Si, respectively ('Pr'). Further details of these composites and composites used by other researchers can be found in Table 1.

For the foaming experiments, all composites were melted in a chamber and foamed by air injection through a stainless steel cannula of 500 µm outer and 200 µm inner diameter. A detailed description of the setup and procedure can be found elsewhere [16]. The temperature of the melt (680 °C) and the air overpressure in the injection line (300 mbar) were kept constant. The foaming process was observed by in-line radioscopy employing a microfocus X-ray source with 5 µm spot size operated at 100 kV and 100 µA and capturing the radiographs on a panel detector with 2240 × 2368 pixels of each 50 × 50 µm2 pixel size [17]. Images were taken every 500 ms. Program "ImageJ" was used to process images, to analyse the foam structure and to determine bubble size and the height of the foam column.

To discuss the ability of a material to be processed to a foam, the term *foamability* is coined. Alloys and composites in which upon gas injection stable are created and the bubble size distribution is narrow, no notable events of bubble merger are observed and the bubbles pile up continuously to form a foam layer of growing thickness are called *foamable (I)*. If, however, bubbles merge with others during foaming (a.k.a. coalescence), giving rise to a coarser and less uniform bubble size distribution than in the case of foamable alloys and a foam column is formed, however of a limited height, a composite is called only *partially foamable (II)*. If bubbles lose gas or collapse immediately after reaching the melt surface and disappear or form a characteristic onion-shaped structure of bubble remnants a composite is deemed *unfoamable (III)*. In Figure 1, the different levels of foamability (I, II, III) are exemplarily shown for foams blown by injecting air into a melt held at 680 °C. The state shown was obtained by injecting for 15 s and holding for 60 s after.

The experiments in this work were performed under the same conditions for all the composites, see Table 1. The levels of foamability obtained are given in the 7th column of the table. The materials investigated by other researchers (see references) might have been manufactured using different equipment and parameters such as injector diameter, gas type, pressures, etc., but the process is fundamentally the same. As particle morphology (spherical or angular), size (diameter D_P = 0.1–1000 µm) and distribution (uniform or agglomerated) can vary notably, a selection of microstructure images of various composites is shown in Figure 2. Examples for spherical particles are f) big SiO_2 (#19 in Table 1) or h) primary Si crystals (#25), whereas angular particles are a) SiC (#1), e) spinel (#18) or g) needle-like primary Fe

crystals (#22). The smallest particles were created in-situ, namely d) using CuO (#16) or e) using SiO_2 (#18), in contrast to the large primary crystals in g) (#22) and h) (#25). All particles show a tendency to agglomerate. An example for distributed particles is seen in a) (#1), one for strongly interconnected TiB_2 particles (#14) encircled in red) in c). Particles created by oxidation are shown in d) (#16) and e) (#18). They not only exhibit a broad particle size distribution but are also prone to agglomeration. Moreover, the initial reactants have not totally transformed to smaller oxides as some residues are still visible.

For a better understanding and to highlight the importance of particle size and particle concentration the two quantities are related in Figure 3. The colour of the symbols and of the background represents the level of stability ranging from a foamable (I, green) over a partially foamable (II, yellow) to an unfoamable (III, red) foam structure. Obviously, a preferable range of foamable composites exists for intermediate particle sizes and concentrations.

Such a diagram has been presented in an early patent to illustrate the possible parameter field for successful foaming of aluminium alloys, however without giving the experimental background. The original diagram was given for an Al-SiC composite and an optimal particle-size / concentration range (3−25 vol% / 0.4−30 µm) was found [6]. The dashed lines in Figure 3 indicate the stability limits claimed there for SiC. In the current work, we show that these limits not only apply to SiC particles but also to other foam stabilising particles investigated here and by other authors whenever gas injection drives foaming. In the following we shall discuss the 4 different boundaries separately and offer explanations. Figure 4 provides a visualisation of these cases.

The diagram proposed in Ref. [6] was analysed by Kaptay who found similar border conditions [18]. Considering the first border (A) “difficult to mix”, see Figure 3, he developed an equation to determine the minimum particle diameter ($D_{P,\mathrm{min}}$) by considering the critical kinetic energy (or stirring velocity v, which in our technical limit is $v_{\mathrm{crit.}} = 60\ \mathrm{m\cdot s^{-1}}$) needed to overcome the interfacial force:

$$D_{P,\mathrm{min}} \geq (1-\cos\theta)^2 \frac{3\gamma}{\rho_P v_{\mathrm{crit}}^2}, \qquad (1)$$

where Θ is the wetting angle between the particle and the melt, γ is the surface tension of the melt (0.85 $\mathrm{J\cdot m^{-2}}$) and ρ_P is the (gravimetric) density of the particles. Calculating $D_{P,\mathrm{min}}$ for our setup and exemplarily for Al_2O_3 ($\rho_P = 3950\ \mathrm{kg\cdot m^{-3}}$, $\Theta = 60°$ [19]) leads to a minimum particle

size of around $D_{P,\min}$ = 0.6 µm. This concurs with experimental data as AlSi9Mg0.6 foams cannot be stabilised using Al_2O_3 particles of D_P = 0.1−0.3 µm (#7), but by particles of 0.6 µm diameter (#6), see Table 1 and Figure 2b. For SiC (ρ_P = 3200 kg·m^{-3}, Θ = 27° [19]) $D_{P,\min}$ = 0.4 µm, which also appears realistic as all melts containing particles of $D_P \geq 1$ µm could be foamed [3,7]. A minimal particle size of 0.02 µm for SiO_2 particles (ρ_P = 2700 kg·m^{-3}, Θ = 70° [19]) is also in good agreement with experimental results of spinel, Al_2O_3 and SiO_2 particles. SiO_2 particles sized around 0.01 µm are hard to be immersed properly into a melt and cannot be foamed (#17), whereas melts containing bigger particles (1–10 µm, #18) are foamable. The consequence of adding too small particles to a melt is that the films contain a too low volume fraction and become unstable, see Figure 4a.

On the other side of the size range, the maximum particle size (see Figure 3, region C) can be given by Stoke´s equation, where the particle settling velocity v_{set} is the limiting factor since it increases with particle size D_P [20]

$$D_P = 2\sqrt{\frac{9\mu v_{\text{set}}}{2g(\rho_P - \rho_L)}}. \quad (2)$$

Here, ρ_L is the density of liquid aluminium alloy (ρ_L = 2420 kg·m^{-3} for AlSi9 at 700 °C [21], similar to that of AlSi9Mg0.6) and μ its viscosity (μ = 1.045 mPa·s for AlSi7Mg0.3 at 690 °C [22]). Kaptay assumed a technical limit of v_{set} = 0.02 mm·s^{-1}, leading to a maximal particle size of D_P = 22 µm for Al_2O_3, D_P = 30 µm for SiC and D_P = 50 µm for SiO_2 [18]. These values differ by a factor of 2, which is small considering the size range in Figure 3. All the present results are compatible with these estimates, see Figure 3 and Table 1. For primary crystals (#21–25) no calculated value of D_P can be given as the precipitations are part of the alloy. Clearly, the large particle sizes (200–2000 µm), see Figure 2 g) and h), do not lead to good foamability of the melt. Another factor limiting stability is given by particles with diameters exceeding the typical foam film thickness (Figure 4c), i.e. D_P > 50 µm [7,8,14,23]. Such particles lead to weak foams (I,II) as wetted particles pull the liquid out of the films due to surface tension and cause thinning of regions in between the particles and films eventually break due to the lack of stabilisation.

Considering the upper border value (Figure 3, region B), “too viscous” was found to be the case for SiC particle concentration of 28−30 vol.% for a particle size of 14±9 µm [24]. As the upper limit of the particle volume fraction is not of practical interest (the goal is to reduce the amount of particles) this is not elaborated in much detail here. Figure 4b visualises the

problem of very high melt viscosity, which does not allow for a proper bubble formation. Bubbles might not even detach from the cannula or become too big, which gives rise to thick films and a poor foam structure.

On the contrary, the minimal particle volume fraction (region D) is very relevant as any reduction would improve machinability of the end product, reduce costs of the raw material and simplify production steps. The corresponding explanation in Ref. [18] for “weak foam stability” is based on the assumption of a double particle layer at the gas-liquid interface [25]. Such highly ordered and structured particle layers could not be found in foams created by gas injection, see Figure 2 and Refs. [3,13,16], which is why this analytical approach cannot be used directly for real foams. Some particles rather tend to segregate to the gas-liquid interfaces and align, others agglomerate or distribute over the entire width of the film. Nevertheless, especially particles situated at the gas-liquid interfaces seem to play an important role and might reduce capillary forces and inhibit drainage. Such particles are found to be pinned to the interface by a continuous oxide skin, which is necessary to stabilise a film. This skin has to be thick and strong enough to hold particles [16]. Particle bridges might be indeed possible from one bubble surface to another and provide a mechanical disjoining force as suggested by Kaptay [25]. So if the minimal particle concentration is not reached (Figure 4d) nothing prevents the bubble surfaces from merging when the film thickness becomes undercritical. If, however, the criteria for particle size and fraction are met the particle configuration might be as shown in Figure 4e.

Air was injected into various aluminium alloy composites to investigate their ability to form liquid metal foam.

- Three different levels of foamability - foamable, partially foamable and unfoamable - were introduced to describe the quality of a foam produced by gas injection.
- It was found that only intermediate particle sizes and concentrations enable foaming by gas injection.
- These limits were found to be similar for different particle types (different compositions and manufacturing routes) and morphologies.
- Four different border conditions delimiting particle sizes and concentrations were discussed in the context of the experimental results.

Table 1. Composites used for gas injection experiments in this work (entries in bold letters) and some data found in the literature.

#	Alloy [wt.%]	particle type extrinsic (Ex) intrinsic (In) primary crystals (Pr)	particle fraction [vol.%]	particle size [µm]	wetting angle [°]	stability foamable (I) partially foamble (II) unfoamable (III)	source	figure
1	**AlSi9Mg0.6**	**SiC (Ex)**	**8**	**10**	**27**	**I**	**this work**	**2a**
2	**AlSi9Mg0.6**	**SiC (Ex)**	**20**	**10**	**27**	**I**	**this work [3,6,7]**	**1a**
3	Al	SiC (**Ex**)	10−20	10−15	27	I	[1]	
4	AlSi10Cu3Ni1.5	SiC (**Ex**)	20	13	27	I	[5]	
5	Al-Si + rare earth	SiC (**Ex**)	8−15	1/7/14/20	27	I	[12]	
6	**AlSi9Mg0.6**	**Al_2O_3 (Ex)**	**10**	**0.6**	**60**	**I**	**this work**	**2b**
7	**AlSi9Mg0.6**	**Al_2O_3 (Ex)**	**10**	**0.1−0.3**	**60**	**III**	**this work**	**1c**
8	AlSi9MgMn (A365)	Al_2O_3 (**Ex**)	3−8	9/15/23	60	I	[13]	
9	AlSi10Mg	Al_2O_3 (**Ex**)	12.5	23	60	I	[5]	
10	AlMg1SiCu	Al_2O_3 (**Ex**)	10	11	60	I	[5–7]	
11	AlSi10Cu3Ni1.5	Al_2O_3 (**Ex**)	10	11	60	I	[5–7]	
12	AlSi10Cu3Ni1.5Mg3	Al_2O_3 (**Ex**)	10	11	60	I	[5–7]	
13	Al-Si + rare earth	Al_2O_3 (**Ex**)	11−20	3.5/5/10	60	I	[12]	
14	**AlSi9Mg0.6**	**TiB_2 (In)**	**6**	**1−3**	**0**	**I**	**this work**	**2c**
15	Al 99.98	TiC (Ex)	4	0.2	10	III	[3]	
16	**AlSi9Mg0.6**	**spinel, Al_2O_3 (In) & CuO (Ex)**	**2.5**	**1–10**	**60**	**II**	**this work**	**1b, 2d**
17	**AlSi9Mg0.6**	**spinel, Al_2O_3 (In) & SiO_2 (Ex)**	**0.2**	**0.01**	**70**	**III**	**this work**	
18	**AlSi9Mg0.6**	**spinel, Al_2O_3 (In) & SiO_2 (Ex)**	**5**	**1–10**	**70**	**II**	**this work**	**2e**
19	**AlSi9Mg0.6**	**SiO_2 (Ex)**	**20**	**100−400**	**70**	**III**	**this work**	**2f**
20	**AlSi9Mg0.6**	**CaO (In)**	**1.5**	**-**	**n.a.**	**II**	**this work**	
21	**AlSi9Fe3Mg0.6**	**Fe (Pr)**	**1**	**100–2000**	**0**	**III**	**this work**	
22	**AlSi9Fe3Mg0.6Cr0.5**	**Fe (Pr)**	**1**	**100–500**	**0**	**III**	**this work**	**2g**
23	**AlSi9Fe3Cr2Mg0.6**	**Fe (Pr)**	**1**	**50–300**	**0**	**II**	**this work**	
24	**AlSi20Mg0.6**	**Si (Pr)**	**19**	**200**	**0**	**II**	**this work**	
25	**AlSi20Mg0.6Ca0.2**	**Si (Pr)**	**19**	**500**	**0**	**III**	**this work**	**2h**

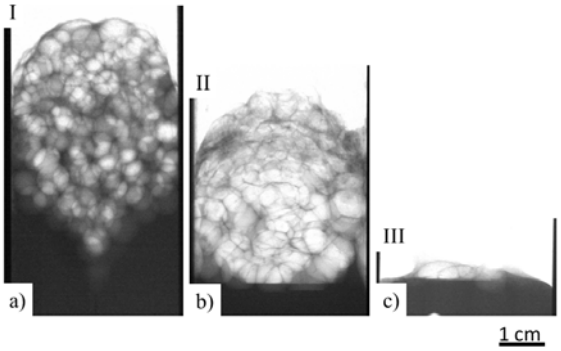

Figure 1. X-ray radioscopies of structures obtained by foaming (or attempting to foam) a) foamable composite AlSi9Mg0.6 + 20 vol.% SiC (D_P ~10 µm), b) partially foamable composite AlSi9Mg0.6 + 2.5 vol.% Al_2O_3 + spinel (intrinsic composite created by oxidation using CuO), c) unfoamable composite AlSi9Mg0.6 + 10 vol.% Al_2O_3 (D_P = 0.1−0.3 µm). All composites were blown with air for 15 s injection, after which the melt was held for 60 s at 680 °C.

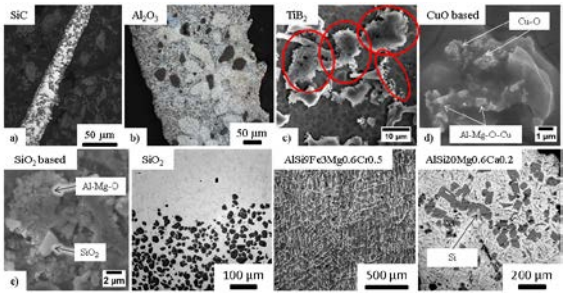

Figure 2. Composites based on various matrix alloys containing extrinsic (Ex) or intrinsic (In) particles or primary crystals (Pr): a) SiC (Ex), b) Al_2O_3 (Ex), c) TiB_2 (In)*, d) spinel/CuO (In)*, e) spinel/SiO_2 (In)*, f) SiO_2 (Ex), g) Fe-rich crystals (Pr) and h) Si-rich crystals (Pr). Reactants (e.g. oxidants) and particles are highlighted in some cases. All images marked with an asterisk are SEM images, the others light optical micrographs. In Table 1 the images are linked to the type of composite.

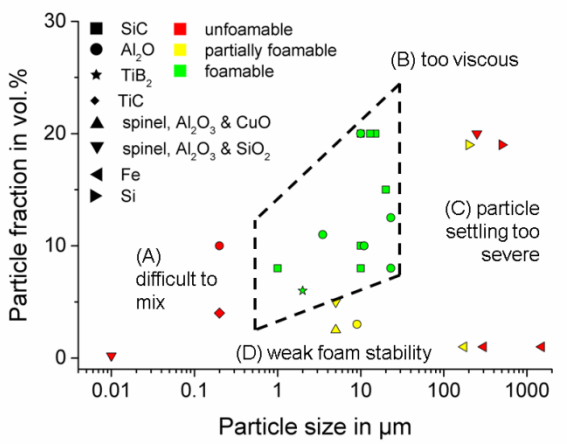

Figure 3. Foam stability diagram showing the level of foamability for different combinations of particle size and particle volume fraction. Green symbols represent a foamable (I), yellow a partially foamable (II) and red an unfoamable (III) composite. Each symbol represents one of the 25 entries in Table 1 and the dashed frame the outer stability boundaries for AlSi+SiC foams as suggested in the literature [6].

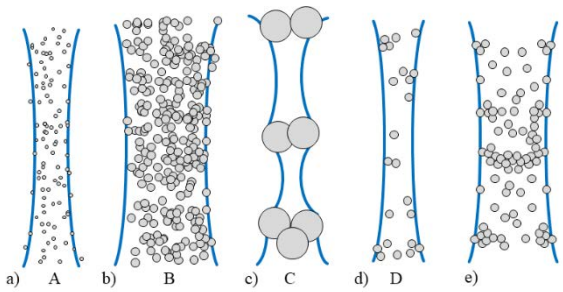

Figure 4. Schematic of particle distributions in a liquid film. Various configurations related to the four borders in Figure 3 are shown. a) Too small particles and difficult to mix (A), b) Fluid too viscous (B), c) Particles too large and settling too severe (C), Too few particles (D). e) Optimal configuration for the present system (trapezium of Figure 3).

References

[1] M. A. De Meller, French Patent 615,147 (1925) 1926.

[2] J. Banhart, Adv. Eng. Mater. 15 (2013) 82.

[3] S. W. Ip, Y. Wang, J. M. Toguri, Can. Metall. Quart. 38 (1999) 81.

[4] A. Haibel, A. Rack, J. Banhart, Appl. Phys. Lett. 89 (2006) 154102.

[5] C. Körner, M. Arnold, R. Singer, Mater. Sci. Eng. A. 369 (2005) 28.

[6] I. Jin, L. D. Kenny, H. Sang, USA Patent 4,973,358 (1989) 1990.

[7] D. Q. Wang, Z. Y. Shi, Mater. Sci. Eng. A. 361 (2003) 45.

[8] D. Leitlmeier, H. P. Degischer, H. J. Flankl, Adv. Eng. Mater. 4 (2002) 735.

[9] N. Babcsán, D. Leitlmeier, H.-P. Degischer, J. Banhart, Adv. Eng. Mater. 6 (2004) 421.

[10] F. García-Moreno, B. Siegel, K. Heim, A. J. Meagher, J. Banhart, Colloid Surface A. 437 (2015) 60.

[11] N. Babcsán, F. Garcia-Moreno, J. Banhart, Colloid Surface A. 309 (2007) 254.

[12] K. Kadoi, N. Babcsán, H. Nakae, Mater. Sci. Forum. 649 (2010) 385.

[13] N. Babcsán, J. Banhart, Towards High-Temperature Colloid Chemistry, in: B. P. Binks, T. S. Horozov (Eds.), Colloidal particles at liquid interfaces, Cambridge University Press, Cambridge, 2006, pp. 445-500.

[14] N. Babcsán, D. Leitlmeier, H. P. Degischer, Materialwiss. Werkst. 34 (2003) 22.

[15] K. Heim, G. S. Vinod-Kumar, F. Garcia-Moreno, J. Banhart, J. Mater. Sci. 52 (2017) 6401.

[16] K. Heim, G. S. Vinod-Kumar, F. García-Moreno, A. Rack, J. Banhart, Acta Mater. 99 (2015) 313.

[17] F. García-Moreno, N. Babcsán, J. Banhart, Colloid Surface A. 263 (2005) 290.

[18] G. Kaptay, A generalised stability diagram of production of metallic foams by the melt route, in: J. Banhart, N. A. Fleck, M. F. Ashby (Eds.), Cellular Metals and Metal Foaming Technology, Verlag MIT Publishing, 2001, pp. 117-122.

[19] G. Kaptay, E. Bader, B. Bolyan, Mater. Sci. Forum. 329-330 (2000) 151.

[20] G. S. Kumar, B. S. Murty, M. Chakraborty, Inter. J. Cast. Met. Res. 23 (2010) 194.

[21] E. Gebhardt, D. K., Z. Metallk. 50 (1959) 379.

[22] D. Wang, R.A. Overfelt, Int. J. Thermophys. 23 (2002) 1063.

[23] X. N. Liu, Y. X. Li, X. Chen, Y. Liu, X. L. Fan, J. Mater. Sci. 45 (2010) 6481.

[24] G. A. Irons, K. Owusu-Boahen, Metall. Mater. Trans. B. 26 (1995) 981.

[25] G. Kaptay, Colloid Surface A. 230 (2004) 67.